Biochemistry

pubs.acs.org/biochemistry Article

Mutagenesis, Hydrogen−Deuterium Exchange, and Molecular Docking Investigations Establish the Dimeric Interface of Human Platelet-Type 12-Lipoxygenase

Wan-Chen Tsai,[#] Ansari Mukhtar Aleem,[#] Chris Whittington, Wilian A. Cortopassi, Chakrapani Kalyanaraman, Angel Baroz, Anthony T. Iavarone, Ewa Skrzypczak-Jankun, Matthew P. Jacobson, Adam R. Offenbacher,* and Theodore Holman*

Cite This: *Biochemistry* 2021, 60, 802−812 Read Online

ACCESS | Metrics & More | Article Recommendations | Supporting Information

ABSTRACT: It was previously shown that human platelet 12*S*-lipoxygenase (h12-LOX) exists as a dimer; however, the specific structure is unknown. In this study, we create a model of the dimer through a combination of computational methods, experimental mutagenesis, and hydrogen−deuterium exchange (HDX) investigations. Initially, Leu183 and Leu187 were replaced by negatively charged glutamate residues and neighboring aromatic residues were replaced with alanine residues (F174A/W176A/L183E/L187E/Y191A). This quintuple mutant disrupted both the hydrophobic and $\pi-\pi$ interactions, generating an h12-LOX monomer. To refine the determinants for dimer formation further, the L183E/L187E mutant was generated and the equilibrium shifted mostly toward the monomer. We then submitted the predicted monomeric structure to protein−protein docking to create a model of the dimeric complex. A total of nine of the top 10 most energetically favorable docking conformations predict a TOP-to-TOP dimeric arrangement of h12-LOX, with the α-helices containing a Leu-rich region (L172, L183, L187, and L194), corroborating our experimental results showing the importance of these hydrophobic interactions for dimerization. This model was supported by HDX investigations that demonstrated the stabilization of four, non-overlapping peptides within helix α2 of the TOP subdomain for wt-h12-LOX, consistent with the dimer interface. Most importantly, our data reveal that the dimer and monomer of h12-LOX have distinct biochemical properties, suggesting that the structural changes due to dimerization have allosteric effects on active site catalysis and inhibitor binding.

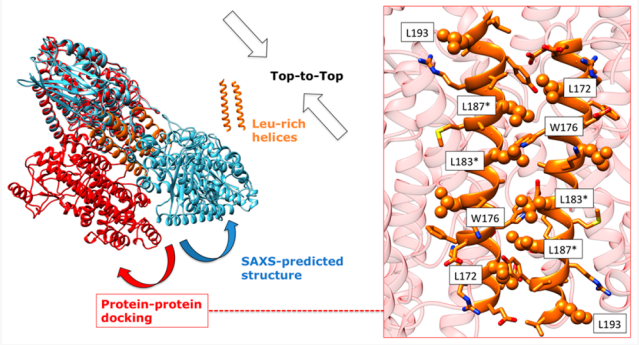

Human platelet 12*S*-lipoxygenase (h12-LOX or ALOX12) adds molecular oxygen at C-12 of arachidonic acid (AA) with *S* chirality to generate 12(*S*)-hydroperoxyeicosatetraenoic acid [12*S*-HpETE].[1−3] This hydroperoxide is subsequently reduced by glutathione peroxidase to yield 12(*S*)-hydroxyeicosatetraenoic acid [12*S*-HETE].[4−7] These h12-LOX products, as well as others from different fatty acids, influence platelet aggregation and play a role in many inflammatory diseases,[8] such as psoriasis,[9] diabetes,[10−12] and cancer,[13−18] indicating h12-LOX as a possible therapeutic target.[8,19,20] Currently, the main effort in the search for inhibitors targeting lipoxygenases has been directed to the active site, blocking the direct enzymatic activity of fatty acid peroxidation. However, allosteric inhibition may also be relevant, as seen for cyclooxygenase (COX).[21,22]

The first high-resolution crystal structure of mammalian lipoxygenase, rabbit 15*S*-LOX-1 (r15-LOX-1, r12/15-LOX, or rALOX15), was reported as a dimer,[23] although its interface was not correctly described until 10 years later.[24] It took another 5 years until it was postulated that monomeric r15-LOX-1 becomes a dimer in the presence of 13*S*-hydroxyoctadeca-9*Z*,11*E*-dienoic acid (13-HODE), the reduced form of its endogenous hydroperoxide product, 13-HpODE.[25] Monomeric r15-LOX-1 has also been used as a homology model for other lipoxygenases, with the TOP being defined as a subdomain region from residue 163 to 222, covering the active site in the helical bundle of the catalytic domain. Although the crystal structures suggest oligomers for some lipoxygenases, the nature of their association has not been discussed,[26−29] except for h12-LOX[30] and coral 11R-LOX (c11-LOX),[31] which were reported to be stable and active as dimers. There is no crystal structure of an active, full-length

Received: January 19, 2021
Revised: February 12, 2021
Published: February 26, 2021

Downloaded via GEORGIA INST OF TECHNOLOGY on May 6, 2022 at 16:16:14 (UTC).
See https://pubs.acs.org/sharingguidelines for options on how to legitimately share published articles.

© 2021 American Chemical Society

https://dx.doi.org/10.1021/acs.biochem.1c00053
Biochemistry 2021, 60, 802−812

h12-LOX; however, wild-type (wt) h12-LOX has been shown experimentally to agglomerate into large clusters,[30] and there are indications that other human lipoxygenases might not be monomeric either.[32] Previously, Shang and co-workers used a combination of thermodynamic calculations, thermal motion analysis, and results of small-angle X-ray analysis (SAXS) to propose a dimeric structure of h12-LOX connected in a TOP-to-TOP fashion (Figure 1), defined by interactions between

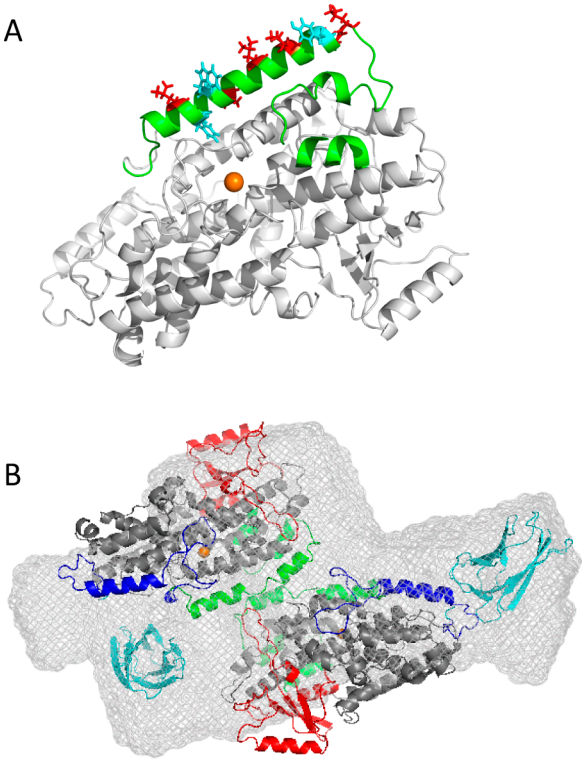

Figure 1. (A) Homology model of the wt-h12-LOX catalytic domain with the TOP region (residues 163−222) colored green. Leucines in this region are colored red, and aromatic amino acids cyan. (B) TOP-to-TOP model (the SAXS-predicted structure from our earlier publication).[30] The color legend is as follows: cyan, PLAT domain (residues 1−110); blue, linker (residues 111−162); green, TOP domain (residues 163−222); red, PDZ domain (residues 223−333); gray, remaining catalytic domain (residues 334−663); orange sphere, iron center.

their α2 helices.[33] The assembly of dimers via the α2 helices, running in opposite directions (antisymmetric), has been tested in r15-LOX-1 by site-directed mutagenesis and SAXS, supporting a model in which such dimers, as found in its crystal structure,[24] are stabilized by a leucine zipper motif formed by L179A ↔ L192B and L183A ↔ L188B interactions, where A and B stand for monomer A and monomer B, respectively.[25] However, the dimerization interaction for coral 11R-LOX was determined to be through its PDZ-like domain.[31] Although a similar PDZ-like domain interaction for h12-LOX was predicted by thermodynamic stability calculations, a model of dimerization through this domain was inconsistent with SAXS analysis[30,33] and thus was rejected as a possible dimer structure model. In the work presented here, the results from site-directed mutagenesis, *in silico* modeling, and hydrogen−deuterium exchange mass spectrometry (HDX-MS) suggest a TOP-to-TOP h12-LOX dimerization model that is mediated by an interaction similar to a leucine zipper.

MATERIALS AND METHODS

Chemicals. Fatty acids used in this study were purchased from Nu-Chek Prep, Inc. Deuterium oxide (99.9%) was purchased from Cambridge Isotope Laboratories (Tewksbury, MA). All other solvents and chemicals were of reagent grade or better and were used as purchased without being further purified.

Homology Model of h12-LOX. A crystal structure of h12-LOX is available in the Protein Data Bank (PDB entry 3D3L, resolution of 2.6 Å); however, this structure is not suitable for the present modeling due to several missing residues. For instance, helix α11 that forms the entrance to the active site is missing. Also, the entire PLAT domain and helix α2, which is positioned parallel to helix α11 in the r15-LOX-1 and porcine 12-LOX structures, is reoriented horizontally above the active site entrance in the h12-LOX structure (structural superposition is shown in Figure S1). Finally, the C-terminal residue, I663, which coordinates the active site ferric ion, is replaced by a heavy construct vector that was not removed. For these reasons, a homology model of h12-LOX (Uniprot accession number P18054) was constructed on the basis of the porcine 12-LOX structure (PDB entry 3rde, resolution of 1.9 Å) using PRIME (version 4.7, Schrödinger Inc.). During homology modeling, we retained the metal ion (Fe^{3+}), a hydroxide ion that coordinated the metal ion, and the co-crystallized ligand, 3-{4-[(tridec-2-yn-1-yloxy)methyl]phenyl}-propanoic acid, from the porcine 12*S*-LOX structure. The h12-LOX model was subsequently energy minimized using Protein Preparation Wizard (Schrödinger Inc.). During the protein preparation step, hydrogen atoms were optimized to make better hydrogen bonding interactions and all heavy atoms were relaxed such that they did not move more than 0.3 Å from their starting position. After the protein preparation step, we separated the protein and the co-crystallized ligand into two separate entries in the Maestro project table. The protein entry included metal (Fe^{3+}) and hydroxide ions.

Site-Directed Mutagenesis. To test the TOP-to-TOP model of dimerization in h12-LOX, site-directed mutagenesis was employed to introduce mutations into this region that would abolish the hypothesized hydrophobic and $\pi-\pi$ interactions. The following two mutations were introduced: F174A/W176A/L183E/L187E/Y191A and L183E/L187E. We follow the same residue numbering convention that is used in UniProt for the h12-LOX sequence (accession number P18054). The Online QuikChange Primer Design tool (http://www.genomics.agilent.com/primerDesignProgram.jsp) from Agilent Technologies (Santa Clara, CA) was used to design the primers for all of the mutants of h12-LOX. The mutations were introduced using a QuikChangeII XL site-directed mutagenesis kit from Agilent Technologies by following the instructions in the provided protocol. The mutations were confirmed by sequencing the LOX insert in the pFastBac1 shuttle vector (Eurofins Genomics).

Protein Expression and Purification. The expression and purification of h12-LOX and mutant enzymes used in this study were performed as previously described.[34,35] The wild-type (wt-h12-LOX) enzyme and its mutants were expressed as fusion proteins with a six-His tag on the N-terminus and purified by affinity nickel-iminodiacetic acid agarose using FPLC (Bio-Rad). The entire purification process was

https://dx.doi.org/10.1021/acs.biochem.1c00053
Biochemistry 2021, 60, 802−812

performed at 4 °C. The purity of all of the proteins was >90%, as determined by sodium dodecyl sulfate−polyacrylamide gel electrophoresis analysis.

Size Exclusion Chromatography. Size exclusion chromatography (SEC) was performed on the affinity-purified proteins using an AKTA Pure system. After centrifugation at 13000 rpm for 5 min (to sediment any debris), the purified protein was loaded onto either a Superdex 200, 10/300 GL column (GE Healthcare) for Figure 2 or a Superdex 75, 10/300 GL column (GE Healthcare) for Figure 3 equilibrated with 25 mM HEPES (pH 7.5) at a flow rate of 0.3 mL/min. The elution volume (V_e) for Figure 2 was compared with that of the gel filtration standard (Bio-Rad, catalog no. 151-1901) containing horse thyroglobulin (670 kDa), bovine γ-globulin (158 kDa), chicken ovalbumin (44 kDa), horse myoglobin (17 kDa), and vitamin B_{12} (1.35 kDa), and the elution volume (V_e) for Figure 3 was compared with the Protein Standard Mix 15−600 kDa (Sigma-Aldrich), containing horse thyroglobulin (670 kDa), bovine γ-globulin (158 kDa), chicken ovalbumin (44 kDa), bovine pancreatic ribonuclease (13.7 kDa), and pABA (0.14 kDa). A standard curve of MWs relative to elution volume was utilized to establish monomeric and dimeric h12-LOX (Figure S3).

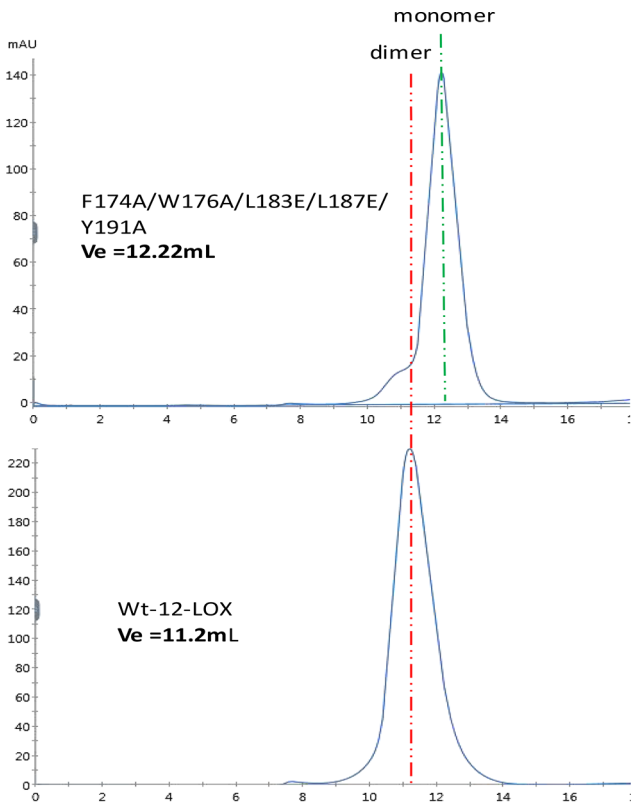

Figure 2. Size exclusion chromatogram of wt-h12-LOX and the F174A/W176A/L183E/L187E/Y191A mutant protein. V_e is the elution volume.

Determination of the Iron Content Using Inductively Coupled Plasma Mass Spectrometry (ICP-MS). The iron content of wt-h12-LOX and all of the mutant enzymes was determined on a Thermo Element XR inductively coupled plasma mass spectrometer. Cobalt EDTA was used as an internal standard. Iron concentrations were determined by comparison with standardized iron solutions (range of 20−30% occupancy), and all kinetic data were normalized to the iron content. Protein concentrations were determined by a Bradford assay, with bovine serum albumin as the protein standard.

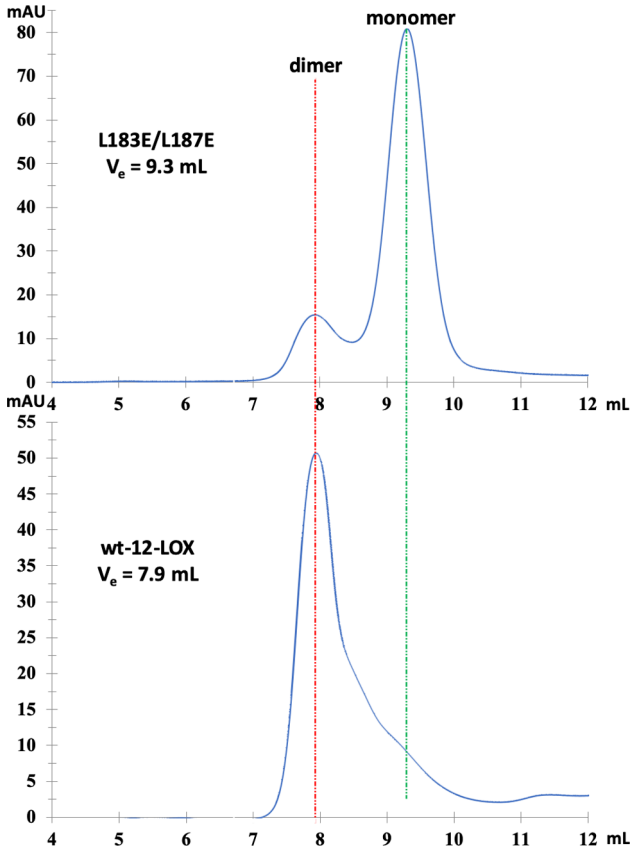

Figure 3. Size exclusion chromatogram of wt-h12-LOX and the L183E/L187E monomer mutant.

Steady-State Kinetics. The wt and mutant h12-LOX enzymatic rates were determined in triplicate by following the formation of the conjugated diene product, 12*S*-HpETE (ε = 25000 M^{-1} cm^{-1}), at 234 nm with a PerkinElmer Lambda 40 UV/vis spectrophotometer. The reactions were started by adding approximately 40 nM enzyme to a 2 mL reaction mixture containing 1−20 μM AA, in 25 mM HEPES buffer (pH 8.00), in the presence of 0.01% Triton X-100, at room temperature (23 °C), while being constantly stirred. The Triton X-100 is added to weaken substrate inhibition. Kinetic data were obtained by recording initial enzymatic rates at each substrate concentration and then fitting them to the Michaelis−Menten equation using the KaleidaGraph (Synergy) program to determine k_{cat} and k_{cat}/K_M values.

Ultraviolet (UV)−Visible-Based IC_{50} Assay. IC_{50} values of ML355, an h12-LOX specific inhibitor,[36] against h12-LOX and its mutants were determined in the same manner as the steady-state kinetic values. The reactions were carried out in 25 mM HEPES buffer (pH 8.00), 0.01% Triton X-100, and 10 μM AA. IC_{50} values were obtained by determining the enzymatic rate at six inhibitor concentrations and plotting them against inhibitor concentration, followed by a hyperbolic saturation curve fit. The data used for the saturation curve fits were performed in duplicate or triplicate, depending on the quality of the data. Triton X-100 is used to ensure proper solubilization of the inhibitor.

https://dx.doi.org/10.1021/acs.biochem.1c00053
Biochemistry 2021, 60, 802−812

Liquid Chromatography-Tandem Mass Spectrometry Analysis of Enzymatic Products. To determine the products formed, wt-h12-LOX and the mutant enzymes were reacted, in triplicate, with 10 μM AA in 25 mM HEPES buffer (pH 7.5) for 10 min. The reactions were quenched with 1% glacial acetic acid, and the mixtures extracted three times with dichloromethane (DCM). The products were then reduced with trimethyl phosphite and evaporated under a stream of nitrogen gas. The reaction products were reconstituted in methanol and analyzed via liquid chromatography-tandem mass spectrometry (LC-MS/MS). Chromatographic separation was performed using a C18 Synergi (4 μM) Hydro-RP 80 Å LC column (150 mm × 2 mm). The injection volume was 20 μL. The chromatography system had a Thermo PDA Plus UV detector, coupled to a Thermo-Electron LTQ mass spectrometer. All analyses were performed in negative ionization mode at the normal resolution setting. Mobile phase A consisted of water with 0.1% (volume/volume) formic acid, and mobile phase B consisted of acetonitrile with 0.1% formic acid. The method ran 60% mobile phase A and 40% mobile phase B initially, then at 30 min decreased the level of mobile phase A to 55% and increased the level of mobile phase B to 45%, and, finally, gradually decreased the percentage of mobile phase A and increased the percentage of mobile phase B until they reached 25% mobile phase A and 75% mobile phase B at 60 min. The flow rate was 200 μL/min. The products were ionized by electrospray ionization. MS/MS was performed in a targeted manner with a mass of 319.5 (for HETE detection). The reaction products were identified by matching their retention times, MS/MS (fragmentation) spectra, and UV spectra to known standards.

***In Silico* Modeling of the Human h12-LOX Dimer.** TheZDock protein−protein docking server[37] was used to predict the dimeric structure of h12-LOX. The top 10 most favorable complexes were analyzed, and the lowest-energy docking pose was chosen for further analysis.

HDX-MS Sample Preparation. Aliquots of the h12-LOX monomer or dimer (3 mg/mL) were thawed and diluted 10-fold (5 μL into 45 μL) in 10 mM HEPES, 150 mM NaCl, 5 mM DTT, and pD 7.4 D_2O (99% D) buffer (corrected; pD = pH_{read} + 0.4). Samples were incubated randomly at 10 time points (0, 10, 20, 45, 60, 180, 600, 1800, 3600, and 7200 s) at 25 °C using a water bath. For each h12-LOX variant, the HDX samples were prepared over the course of 3 days and the time points were randomized to reduce the systematic error. Each time point was prepared and processed once. At the designated incubation time, all samples were then treated identically; the samples were rapidly cooled (5−6 s in a −20 °C bath) and acid quenched (to pH 2.4, confirmed with a pH electrode, with a 0.32 M citric acid stock solution to a final concentration of 90 mM). Procedures from this point were conducted near 4 °C. Prior to pepsin digestion, guanidine HCl (in citric acid, pH 2.4) was mixed with the samples to a final concentration of 0.5 M. h12-LOX HDX samples were digested with pre-equilibrated [10 mM citrate buffer (pH 2.4)], immobilized pepsin for 2.5 min. The peptide fragments were filtered, removing the pepsin, using spin cups (cellulose acetate) and by centrifugation for 10 s at 4 °C. Samples were flash-frozen immediately in liquid nitrogen and stored at −80 °C until data were collected.

Liquid Chromatography-Tandem Mass Spectrometry for h12-LOX Peptide Identification. To identify peptide fragments of h12-LOX resulting from pepsin digestion, samples of pepsin-digested h12-LOX at time zero (H_2O buffer) were analyzed using a Thermo Dionex UltiMate3000 RSLCnano liquid chromatography (LC) system that was connected in line with an LTQ Orbitrap XL mass spectrometer equipped with an electrospray ionization (ESI) source (Thermo Fisher Scientific, Waltham, MA). The liquid chromatograph was equipped with a C18 analytical column (Acclaim PepMap 100, length of 150 mm, inner diameter of 0.075 mm, particle size of 3 μm, Thermo). Solvent A consisted of 99.9% water and 0.1% formic acid, and solvent B consisted of 99.9% acetonitrile and 0.1% formic acid (v/v). The elution program consisted of isocratic flow at 2% B for 4 min, a linear gradient to 30% B over 38 min, isocratic flow at 95% B for 6 min, and isocratic flow at 2% B for 12 min, at a flow rate of 300 nL/min. The column exit was connected to the ESI source of the mass spectrometer using polyimide-coated, fused-silica tubing (inner diameter of 20 μm, outer diameter of 280 μm, Thermo). Full-scan mass spectra were acquired in the positive ion mode over the range of m/z 350−1800 using the Orbitrap mass analyzer, in profile format, with a mass resolution setting of 60000 (at m/z 400, measured at full width at half-maximum peak height).

In the data-dependent mode, the eight most intense ions exceeding an intensity threshold of 30000 counts were selected from each full-scan mass spectrum for tandem mass spectrometry (MS/MS) analysis using collision-induced dissociation (CID). Real-time dynamic exclusion was enabled to preclude reselection of previously analyzed precursor ions. Data acquisition was controlled using Xcalibur software (version 2.0.7, Thermo). Raw data were searched against the amino acid sequence of h12-LOX using Proteome Discoverer software (version 1.3, SEQUEST, Thermo) to identify peptides from MS/MS spectra.

Liquid Chromatography−Mass Spectrometry for Hydrogen−Deuterium Exchange Measurements. Deuterated, pepsin-digested samples of monomeric and dimeric h12-LOX were analyzed using a 1200 series liquid chromatograph (Agilent) that was connected in line with the LTQ Orbitrap XL mass spectrometer (Thermo). The liquid chromatograph was equipped with a reversed-phase analytical column (Viva C8, length of 30 mm, inner diameter of 1.0 mm, particle size of 5 μm; Restek, Bellefonte, PA) and guard precolumn (C8, Restek). Solvent A consisted of 99.9% water and 0.1% formic acid, and solvent B consisted of 99.9% acetonitrile and 0.1% formic acid (v/v). Each sample was thawed immediately prior to injection onto the column. The elution program consisted of a linear gradient from 5% to 10% B over 1 min, a linear gradient to 40% B over 5 min, a linear gradient to 100% B over 4 min, isocratic conditions at 100% B for 3 min, a linear gradient to 5% B over 0.5 min, and isocratic conditions at 5% B for 5.5 min, at a flow rate of 300 μL/min. The column compartment was maintained at 4 °C and lined with towels to absorb atmospheric moisture condensation. The column exit was connected to the ESI source of the mass spectrometer using PEEK tubing (inner diameter of 0.005 in., outer diameter of 1/16 in., Agilent). Mass spectra were acquired in the positive ion mode over the range of m/z 350−1800 using the Orbitrap mass analyzer, in profile format, with a mass resolution setting of 100000 (at m/z 400). Data acquisition was controlled using Xcalibur software (version 2.0.7, Thermo).

Mass spectral data acquired for HDX measurements were analyzed using the software, HDX Workbench.[38] The percent

https://dx.doi.org/10.1021/acs.biochem.1c00053
Biochemistry 2021, 60, 802−812

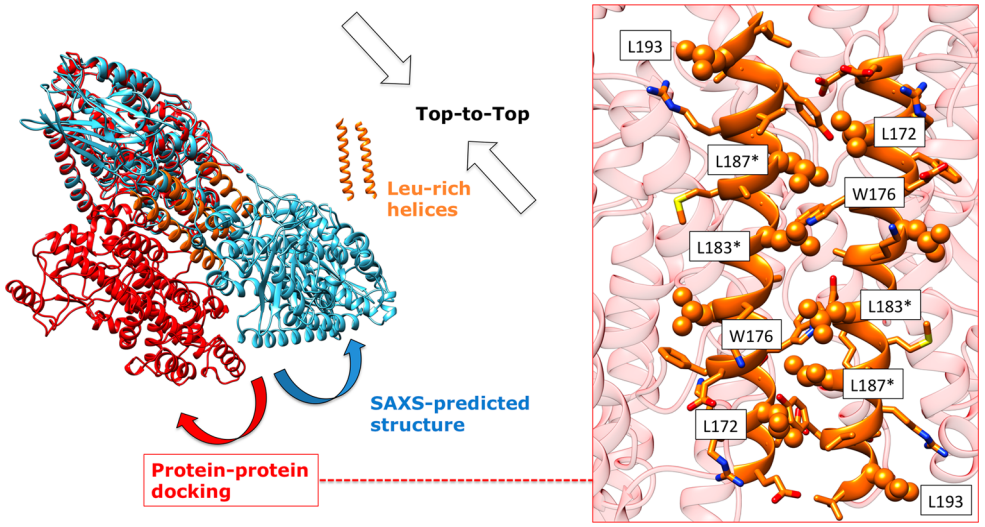

Figure 4. Superimposition of the predicted TOP-to-TOP models of the dimeric structure of h12-LOX from protein−protein docking (red) and SAXS data (blue). In spite of both models showing Leu-rich α-helices (orange) at the interface of the dimerization domain, differences in the overall conformation of the predicted structures are observed, with the protein−protein docking predicted model presenting a higher degree of surface complementarity. The docking and SAXS data suggest two potential binding modes; they differ in the exact interface of the protein−protein interaction, but both of them highlight the favorability of the TOP-to-TOP conformation. Leucine residues are shown as balls and sticks, while other residues in the helices are shown as sticks. Asterisks denote mutation sites in this work.

deuterium incorporation was calculated for each of these peptides, taking into account the number of amide linkages (excluding proline residues) and the calculated number of deuterons incorporated. The values were normalized for 100% D_2O and corrected for peptide specific back-exchange, HDX% = [observed, normalized extent of deuterium incorporation (in percent)]/(1 − BE/100).[39]

Peptide specific back-exchange was determined by fully exchanging the h12-LOX-derived peptides in 100% D_2O, quenching with deuterated acid and performing HDX-MS measurement to determine the extent of the reverse exchange (N−D → N−H). Peptides of h12-LOX were generated from pepsin digestion as described above, but in H_2O buffer. Water was subsequently removed by lyophilization. The peptide mixture was dissolved in buffered D_2O (pD 9), incubated at 90 °C for 2 h in a sealed microcentrifuge tube, and then quenched to pD 2.5 using dilute DCl (Cambridge Isotope Laboratories). The sample was frozen in liquid nitrogen and stored at −80 °C until HDX analysis. The extent of deuterium incorporation in this sample was analyzed via LC-MS as described above for HDX. Back-exchange values ranged from 2% to 50%, for an average value of 20% (see the HDX Summary Table). The resulting data were plotted as deuterium exchange versus time using Igor Pro software (see HDX plots).

RESULTS AND DISCUSSION

TOP-to-TOP Model of Dimerization in h12-LOX. Previously, it was demonstrated that h12-LOX existed as a dimer, which was easily converted to larger aggregates.[30] This could be controlled by mutating surface-exposed Cys residues to Ser, but not totally eliminated.[30,32] Furthermore, following SAXS analysis and modeling, Shang and co-workers predicted a TOP-to-TOP model of dimerization of h12-LOX (Figure 1B). It should be noted that the TOP is a subdomain region of h12-LOX (residues 163−222), as depicted in Figure 1. This region has many leucines (L172, L178, L183, L187, L193, and L194) that could provide hydrophobic interactions between the monomers. Also present in this region are aromatic amino acids, F174, W176, and Y191, that could form $\pi-\pi$ interactions at the dimer interface. To test this model, a mutant was made in which the leucines at position 183 and 187 were replaced with negatively charged glutamates and the neighboring aromatic residues were replaced with alanine residues (F174A/W176A/L183E/L187E/Y191A), to disrupt both the hydrophobic and $\pi-\pi$ interactions. Size exclusion chromatography was performed, and the mutant protein eluted as a monomer (Figure 2), supporting our hypothesis that h12-LOX dimerizes in TOP-to-TOP fashion.

Leucine Interactions Responsible for Dimerization. Having successfully disrupted the h12-LOX dimer using five mutations, we further investigated specific interactions of the dimer interface. In the r15-LOX-1 crystallographic dimer, leucines at positions 179, 183, 188, and 192 form a hydrophobic cluster, contributing to the dimer interface (L179A ↔ L192B and L183A ↔ L188B, where A and B stand for monomer A and monomer B, respectively). Introduction of negatively charged residues (W181E + H585E and L183E + L192E) at the intermonomer interface disturbed the hydrophobic dimer interaction of r15-LOX-1. In h12-LOX, only two of these leucines are conserved (L178 and L187, corresponding to L179 and L188, respectively, in the rabbit sequence); however, other leucines are present in the vicinity, namely, L183, L193, and L194, that might contribute to this network of hydrophobic interactions. Therefore, the L183E/L187E mutant was made and characterized by SEC to determine the shift of the monomer−dimer equilibrium. As shown in Figure 3 and confirmed by protein standards (Figure S2), L183E/L187E shifted the equilibrium mostly toward the monomer, confirming that exchanging the two leucines of the same polypeptide with glutamates, L183 and L187, disrupts the dimer and indicates that they form leucine A:B pairs at the dimer interface.

***In Silico* Modeling of Human h12-LOX Dimers.** In this work, we created a homology model of the h12-LOX monomer structure and then performed protein−protein docking to create models of the dimeric complex. Nine of the top 10 most

https://dx.doi.org/10.1021/acs.biochem.1c00053
Biochemistry 2021, 60, 802−812

Table 1. Steady-State Kinetics, AA Product Profiles, and ML355 IC_{50} Values of the wt-h12-LOX Dimer and the L183E/L187E Mutant Monomer

protein	K_M (μM)	k_{cat} (s^{-1})	k_{cat}/K_M (μM^{-1} s^{-1})	12*S*-HETE:15*S*-HETE product profile	ML355 IC_{50} (μM)
wt-h12-LOX	2.6 ± 0.4	7.0 ± 0.4	2.7 ± 0.3	100:0	0.43 ± 0.04
L183E/L187E	11 ± 4	2.4 ± 0.5	0.2 ± 0.02	78:22	>100

energetically favorable docking models (Figure S3) predict a TOP-to-TOP dimeric arrangement of h12-LOX, with the α-helices containing a Leu-rich region (L172, L187, L183, and L194) of the different monomeric units interacting with each other by hydrophobic interactions. Although no symmetry was enforced, most of the models could be described approximately as either antisymmetric (head to tail) or symmetric (head to head). On the basis of the mutagenesis alone, we cannot distinguish which arrangement is more likely to be correct, although the previously proposed h12-LOX dimer is antisymmetric. In addition, the lowest-energy predicted dimer demonstrates -CH−π interactions between the side chains of L187 and W176, which may contribute to the stability of the complex. This h12-LOX TOP-to-TOP conformation being stabilized by a network of Leu residues has been previously suggested by SAXS data.[30] It is worth noting, however, that the lowest-energy docking conformation presented an interface with a higher degree of surface complementarity when compared to the dimeric conformation proposed by SAXS data in our previous work, and therefore, these models are not superimposable (Figure 4).

Comparison of Biochemical Properties of the Native Dimer (wt-h12-LOX) versus the Mutant Monomer (L183E/L187E). After the identification of L183 and L187 as critical residues for dimerization, the biochemical differences between the dimer (wt-h12-LOX) and monomer (L183E/L187E) were investigated to determine if dimerization affected the biochemistry of h12-LOX. First, the inhibitory potency of wt-h12-LOX (dimer) and L183E/L187E (monomer) by the potent/selective h12-LOX inhibitor, ML355,[40] was investigated. The results revealed that the inhibitory effect of ML355 against wt-h12-LOX (dimer) was consistent with previous work, with an IC_{50} of 0.43 ± 0.04 μM;[36] however, the inhibitory effect of ML355 against the L183E/L187E mutant monomer was almost completely absent (Table 1). This discovery suggests that the conformational changes related to oligomerization could translate to active site residues and affect the inhibitor binding. Subsequently, the steady-state kinetics were determined for both wt-h12-LOX (dimer) and L183E/L187E (monomer), and it was observed that the kinetics of L183E/L187E was dramatically slower than that of wt-h12-LOX, with the k_{cat}/K_M being 0.2 ± 0.02 s^{-1} μM^{-1} and k_{cat} being 2.4 ± 0.5 s^{-1}, which are 13.5- and 2.9-fold, respectively, slower than that of wt-h12-LOX (dimer) (Table 1). The product profile with AA as the substrate was also examined, and for wt-h12-LOX (dimer), 100% 12*S*-HETE was detected as the only product; however, for L183E/L187E (monomer), both 12*S*-HETE (78 ± 1%) and 15*S*-HETE (22 ± 1%) were detected (Table 1). In previous work, it has shown that r15-LOX-1 dimerization protects the enzyme from kinetic substrate inhibition by shielding the hydrophobic α2 helices.[25] However, for h12-LOX, the dimer and monomer were inactivated at the same level of substrate concentration (Figure S4). This observation is contrary to the r15-LOX-1 results where only the mutant monomers revealed substrate/product inactivation above 5−15 μM but not the dimer. In total, these data indicate that the disruption of the dimeric state of h12-LOX translates into an allosteric effect, through either structural or dynamic changes in the active site, ultimately affecting inhibition, catalysis, and the product profile.

Structural Stability of the h12-LOX Variants Assessed by Circular Dichroism (CD) Spectroscopy. The CD spectrum of the wt-h12-LOX dimer variant (Figure 5, red trace) shows the characteristic line shape for a lipoxygenase fold that is predominantly α-helical. The L183E/L187E mutant has a similar CD spectrum (Figure 5, green trace). The thermal stabilities of these variants were measured from CD variable-temperature mode collected at 220 nm (Figure 5, inset). The resulting melting temperatures, T_ms, were virtually identical (50.0 ± 0.7 °C for WT and 48.9 ± 0.6 °C for L183E/L187E). These data dismiss any significant protein unfolding or destabilization as the origin of the kinetic properties emerging from the substitution of aliphatic leucine for the charged glutamate residues.

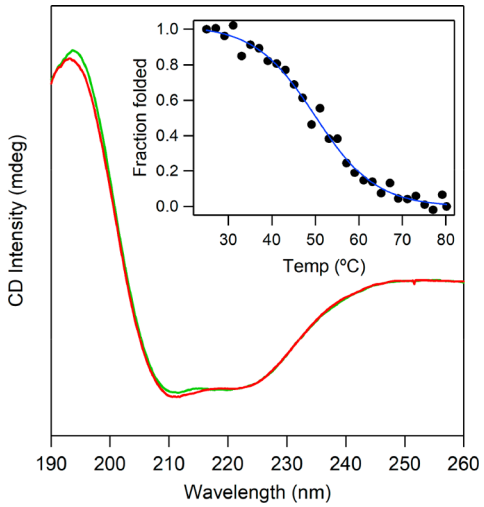

Figure 5. CD spectra of the wt-h12-LOX dimer (green trace) and the L183E/L187E monomer (red trace), recorded at 25 °C. The h12-LOX samples were prepared at concentrations of 1 μM in 25 mM sodium phosphate buffer (pH 7.5). The inset shows a representative temperature-dependent CD melting curve for wt-h12-LOX.

HDX-MS of Wild-Type h12-LOX. In this report, to provide a physical basis for the impact of the L183E/L187E mutation on the protein structure and flexibility that could be linked to the empirical differences in catalytic proficiency, we present comparative HDX-MS performed on wt-h12-LOX (dimer) and the mutant monomer variants. HDX-MS is a powerful tool for investigating protein structure, allostery, and protein−ligand and protein−protein interactions.[39,41−43] Amide backbone N−H bonds that become protected through protein−protein (or dimer) interactions typically undergo slower exchange in the presence of deuterium oxide than solvent-exposed sites. Thus, we anticipated reduced HDX-MS exchange rates at the dimer interface of wt-h12-LOX compared to the mutant monomer.

https://dx.doi.org/10.1021/acs.biochem.1c00053
Biochemistry 2021, 60, 802−812

Tandem MS analysis of pepsin-generated peptides of wt-h12-LOX identified 181 peptides corresponding to 90% coverage of the sequence. For data reduction purposes, 50 non-overlapping peptides, ranging in length from 5 to 28 amino acid residues (average length, 13 residues), were selected for HDX-MS analysis (Figure S5). The peptide list was well covered over all 10 time points, ranging from 10 s to 2 h, and identical for the monomeric form (see below). The percent HDX at three time points was mapped onto the *in silico* model of human 12-LOX (Figure 6). These data provide an important, spatially resolved glimpse into structure and protein flexibility of wt-h12-LOX. While HDX-MS and an X-ray crystal structure of another human LOX, human epithelial 15-LOX-2, have been reported,[29,44] the level of pairwise sequence homology between the isozymes is low (37% identical). It is also important to note that h15-LOX-2 functions as a soluble monomer.

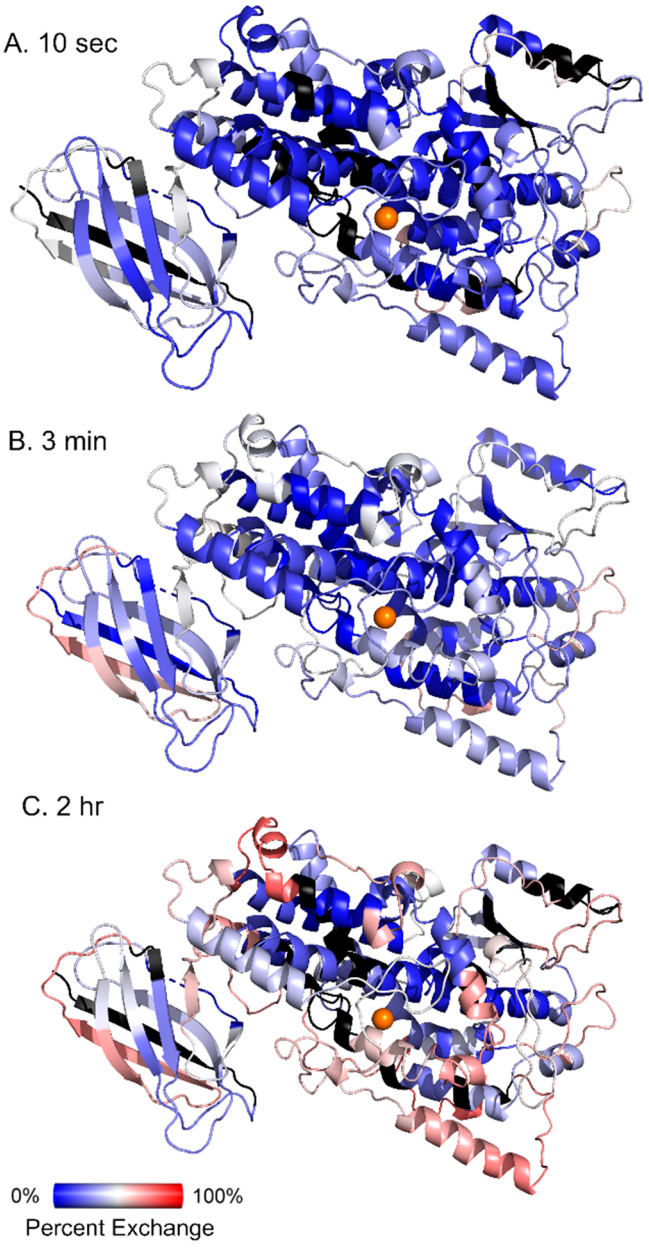

Figure 6. HDX-MS properties of wt-h12-LOX, which exists as a dimer in solution. The coloring is defined by the spectrum bar. Black-colored peptides represent uncovered regions in the mass spectra. All HDX-MS traces can be found in the Supporting Information.

Despite the poor sequence identity, the overall exchange pattern for wt-h12-LOX is similar to that reported for h15-LOX-2 (Figure S6),[44] with one notable and significant distinction in the exchange behavior of helix α2, the central helix in the TOP domain. In h15-LOX-2, the percent exchange is 40−50% at 10 s, 70−80% at 3 min, and nearly complete (80−90%) at 2 h. The exchange pattern for helix α2 in wild-type (dimeric) h12-LOX exhibits a decreased extent of exchange accompanied by a more sluggish apparent rate of exchange. More specifically, the percent exchange values are 20−25%, 30−40%, and 55−65% at 10 s, 3 min, and 2 h, respectively. This difference is functionally relevant as helix α2 lines the putative substrate binding channel and has been proposed to be involved in the allosteric control of substrate binding in 15-LOXs from both plants and mammals.[45] Relevant to the h12-LOX model, proposed herein, it is anticipated that this helix serves as the dimer interface in the wild-type enzyme. The reduced level of exchange of helix α2 in wt-h12-LOX (Figure 7), relative to h15-LOX-2, is consistent with dampened protein flexibility at this helix and with the assignment of the dimer interface (Figure 4).

Identification of the h12-LOX Dimer Interface by HDX-MS: Comparison of the Wild-Type Dimer and Mutant Monomer. Of the non-overlapping peptides (Figure S5), 11 exhibited an at least 6% difference in hydrogen

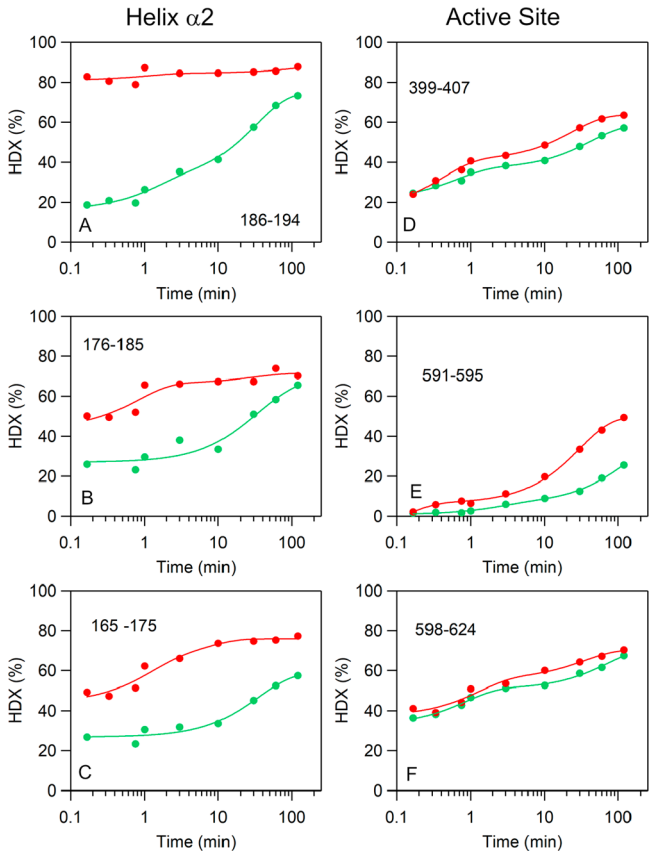

Figure 7. Representative HDX-MS traces that show differences in exchange between the h12-LOX mutant monomer (red trace) and WT dimer (green trace) at (left) helix α2 (site of mutations) and (right) the active site.

https://dx.doi.org/10.1021/acs.biochem.1c00053
Biochemistry 2021, 60, 802−812

exchange extent for at least three time points when the wt-h12-LOX dimer and mutant monomer were compared. Representative peptides illustrating these changes are displayed in Figure 7. The differences were found to be localized at two primary sites, helix α2 of the TOP domain and the active site (Figure 8). In all altered peptides, the mutant monomer (L183E/L187E) exhibited an increased level of exchange in the form of apparent rates and/or extents of HDX.

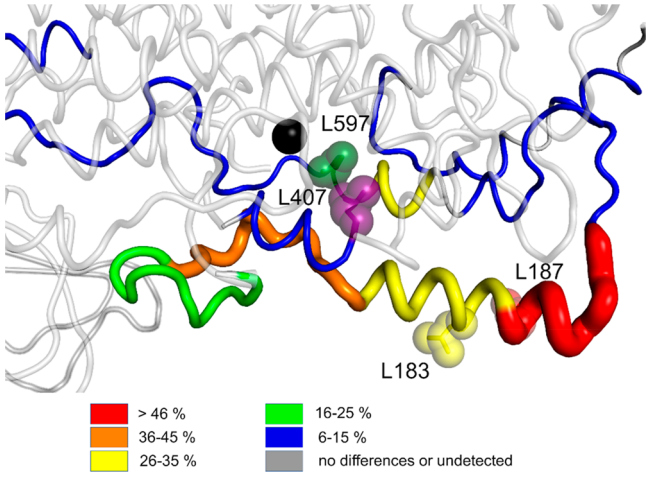

Figure 8. HDX-MS differences between the h12-LOX mutant monomer and wild-type dimer, mapped onto the *in silico* model. The largest degree of HDX differences (in percent) for a given peptide and time is color-coded on the structure by the legend and represented by changes in cartoon putty radii. The residues that mark the site of mutation (L183 → E and L187 → E) are represented as spheres. Helix α2 is bounded by the orange and red amino acids, and the conserved active site leucine residues, L407 and L597, are shown as purple and forest spheres, respectively.

The most dramatic effect in the HDX-MS is seen at the site of the L187 → E mutation (Figure 7A, peptide 186−194). At 10 s, the level of exchange was 18% for dimeric wt-h12-LOX and increased to 83% for the monomeric L183E/L187E mutant. This corresponds to an ∼65% difference in the extent of exchange at this time point; this percent exchange variance is represented as red coloring on the protein model in Figure 8. As the exchange time reaches 2 h, the HDX percent of the dimer increases to 74%, while the level of HDX of the mutant monomer increases only slightly. The nearly complete exchange of this peptide for the monomer at all time points precludes a quantitative analysis for the apparent exchange rates. In addition to this peptide, the adjacent peptide, 176−185, which harbors another mutation (L183E), also showed an enhanced exchange behavior for the mutant monomer. From the multiexponential fits to the data (Figure 7B), the apparent averaged rate of exchange for the mutant was 30-fold faster than that of wt-h12-LOX. Note that mutations, especially nonconserved mutations, can shift the LC retention times that can alter the intrinsic HDX back-exchange values. Indeed, the L → E mutation shifts the LC elution for both peptides, 176−185 and 186−195, from ∼8.4 and ∼7.9 min to ∼7.6 and ∼7.7 min, respectively. To correct for these retention time shifts, back-exchange values were corrected for individual peptides and measured for both wt-h12-LOX and L183E/L187E variants (see the HDX Summary Table). The 176−185 peptide exhibited the largest perturbation in the back-exchange value, from 11.4% in the wild type to 21.4% in the mutant, despite comparable LC retention times.

Importantly, there are two additional peptides (155−164 and 165−175), connected at the N-terminus of peptide 176−185, that do not contain a mutation, yet the HDX-MS behavior between dimeric and monomeric h12-LOX follows that seen for peptide 176−185. These peptides are represented by green and orange coloring, respectively, in Figure 8. Additional overlapping peptides further support these trends (Figure S7). Together, these HDX-MS properties are consistent with enhanced peptide flexibility resulting from loss of dimerization.

In addition to helix α2, the HDX-MS properties of peptides at the active site were also affected (Figure 7D−F). These peptides (396−417, 591−595, and 598−624) are predicted to make direct contact with helix α2, and their backbone flexibility is greatly influenced (i.e., loosened up) by the change in oligomerization. The first example, peptide 396−417, represents the arched helix, which runs parallel to helix α2 and covers the active site pocket. It contains the invariant leucine, L407 (Figure 8, purple spheres), that is located in the hinge region of the U-shaped substrate binding channel. Mutation of this residue to alanine was previously shown to increase the substrate cavity volume and linked to a 100-fold reduction in both the first- and second-order rate constants and a slight shift in AA product distribution.[46] The latter two peptides flank L597 that is located across the binding channel from and proximal to L407. Mutational studies of L597 have not been performed, but the alanine mutation of the orthologous residue in the model 15-LOX from plants (SLO-1), L754A, leads to a 1000-fold decreased k_{cat}.[47] It has been concluded that these two residues are critical for the proper positioning of the substrate with respect to the metallocofactor.[48] While the enzyme activity of these mutations is more compromised than that from the change in oligomerization reported herein, it illustrates how even subtle alterations to the positioning and/or conformational motions of these side chains can be linked to impaired catalytic proficiency. The results further implicate a role for allostery stemming from helix α2 and induced by oligomerization changes that likely accounts for the decreased catalytic proficiency, altered product distribution, and loss of wt-h12-LOX (dimer)-selective inhibitor effects in the case of the monomer.

Note that there are no significant HDX-MS differences observed for peptides located in the h12-LOX PDZ or PLAT domains. The PDZ domain was previously proposed to mediate the dimerization in coral 11*R*-LOX.[31] However, from our data, HDX traces for peptides covering the PDZ domain were identical when the wt-h12-LOX dimer and mutant monomer were compared (for example, see peptides 241−251, 265−273, and 300−315 in HDX plots). Thus, we can rule out the PDZ domain being the site for the dimer interface in wt-h12-LOX. Likewise, HDX-MS properties of peptides in the PLAT domain (residues 1−110), which serves to interact with the phospholipid membrane, are largely unchanged upon mutation of L183 and L187. These data combined with the previously reported SAXS data and our *in silico* model provide compelling support for the antisymmetric arrangement for wt-h12-LOX dimerization, in which the contacts are made along helix α2 of the TOP domain.

We cannot eliminate the possibility that the nonconservative mutations of leucine to glutamate do not contribute to the enhanced flexibility of helix α2. For example, a catalytically

https://dx.doi.org/10.1021/acs.biochem.1c00053
Biochemistry 2021, 60, 802−812

impairing mutant, I553G, of SLO-1 has been shown to influence the flexibility of helix α2 by HDX-MS;[49] however, these effects are relatively modest compared to the drastic effects in HDX that are presented in Figure 7. In addition, the L183E/L187E mutation, presented herein, clearly shifts the oligomerization state from a dimer (WT) to a soluble monomer. The variable-temperature CD measurements also support the conclusion that the mutant does not greatly perturb the protein structure and stability. Together with the lack of any observed HDX differences at the protein surface (other than helix α2), the data support the model presented in Figure 4 in which the dimer interface is formed between the TOP domains and along helix α2.

CONCLUSION

There are experimental data that indicate that h12-LOX exists as a dimer in solution, but because there is no crystal structure of an active, full-length h12-LOX, there is little molecular information about its dimeric interactions. In this work, we demonstrate that mutations of Leu183 and Leu187 to Glu have successfully disrupted the wt-h12-LOX dimer, which suggests dimerization is favored by Leu zippers involving both monomeric units. Recent findings for coral 11*R*-LOX show that leucines in that upper helix impact its stereo- and regiospecificity,[50] which suggests that these hydrophobic residues may have importance in other LOX isozymes, as well. In addition, our protein−protein docking results predict the dimerization of h12-LOX in a TOP-to-TOP orientation, corroborating previous results based on SAXS analysis and *in silico* modeling, with this network of α-helix Leu residues in the dimeric interface.[29] The dimer interaction at helix α2 within the TOP subdomain was validated through HDX-MS results in which enormous enhancements were observed in the apparent rates and the extent of exchange that accompany mutant-induced loss of dimerization. Interestingly, the *in vitro* kinetics and inhibitor profile of monomeric h12-LOX were distinct from those of the dimer, indicating a significant allosteric effect on the active site structure due to dimerization. These observations were supported by our HDX investigations where the enhanced flexibility of helix α2 was accompanied by enhanced flexibility of spatially adjacent active site peptides that are expected to alter the proper positioning of the substrate and inhibitor within the binding pocket.

These data raise the obvious question of the biological role of the h12-LOX dimer in the cell. It is not unusual to observe a conformational change upon protein dimerization, and that conformational interconversion could depend on concentration.[51] Therefore, the dimer could present a structurally distinct species in the cell, affecting protein−protein interactions of h12-LOX, as has been previously postulated with respect to platelet activation.[52] It is also possible that having two membrane association domains in the proximity, which occurs in the dimer, could enhance membrane association of h12-LOX in the cell. Finally, the biological activity of the h12-LOX dimer could depend on its ability to form a heterodimer. The iron content in h12-LOX samples is not always tested and is very seldom mentioned. Our own results and the results reported by others[35,53,54] show that the iron content varies from 0.01 to 0.67 iron atom per molecule of h12-LOX. This means there is always a mixture of catalytically active molecules (E_{cat}) and inactive molecules that do not contain iron (E_{apo}), which could form a heterodimer (E_{cat}:E_{apo}). Heterodimers have been observed in the COX isozymes,[21] where E_{apo} acts as an allosteric domain and therefore h12-LOX may also function as a heterodimer in a similar manner. We are currently investigating all of these possibilities with h12-LOX, in the hopes of understanding the biological role of the dimer further and possibly developing inhibitors against this function.

ASSOCIATED CONTENT

Supporting Information

The Supporting Information is available free of charge at https://pubs.acs.org/doi/10.1021/acs.biochem.1c00053.

HDX Summary Table (XLSX)
HDX plots (PDF)
SEC, molecular dynamics, and HDX (PDF)

Accession Codes

h12-LOX, P18054.

AUTHOR INFORMATION

Corresponding Authors

Theodore Holman − *Department of Chemistry and Biochemistry, University of California, Santa Cruz, Santa Cruz, California 95064, United States;* orcid.org/0000-0001-8072-2959; Phone: +1-831-459-5884; Email: holman@ucsc.edu

Adam R. Offenbacher − *Department of Chemistry, East Carolina University, Greenville, North Carolina 27858, United States;* orcid.org/0000-0001-6990-7178; Phone: +1-252-737-5422; Email: offenbachera17@ecu.edu

Authors

Wan-Chen Tsai − *Department of Chemistry and Biochemistry, University of California, Santa Cruz, Santa Cruz, California 95064, United States*

Ansari Mukhtar Aleem − *Department of Chemistry and Biochemistry, University of California, Santa Cruz, Santa Cruz, California 95064, United States*

Chris Whittington − *Department of Chemistry, East Carolina University, Greenville, North Carolina 27858, United States*

Wilian A. Cortopassi − *Department of Pharmaceutical Chemistry, School of Pharmacy, University of California, San Francisco, San Francisco, California 94143, United States*

Chakrapani Kalyanaraman − *Department of Pharmaceutical Chemistry, School of Pharmacy, University of California, San Francisco, San Francisco, California 94143, United States*

Angel Baroz − *Department of Chemistry and Biochemistry, University of California, Santa Cruz, Santa Cruz, California 95064, United States*

Anthony T. Iavarone − *QB3/Chemistry Mass Spectrometry Facility, University of California, Berkeley, Berkeley, California 94720, United States*

Ewa Skrzypczak-Jankun − *Department of Urology, University of Toledo, Toledo, Ohio 43614, United States*

Matthew P. Jacobson − *Department of Pharmaceutical Chemistry, School of Pharmacy, University of California, San Francisco, San Francisco, California 94143, United States;* orcid.org/0000-0001-6262-655X

Complete contact information is available at: https://pubs.acs.org/10.1021/acs.biochem.1c00053

Author Contributions

#W.-C.T. and A.M.A. contributed equally to this work.

https://dx.doi.org/10.1021/acs.biochem.1c00053
Biochemistry 2021, 60, 802−812

Funding

Supported by National Institutes of Health (NIH) Grant AG047986 (T.H.), National Science Foundation Grant 2003956 (A.R.O.), and NIH Grant 1S10 OD020062 (QB3/Chemistry Mass Spectrometry Facility at the University of California, Berkeley).

Notes

The authors declare the following competing financial interest(s): M.P.J. is a consultant to and shareholder of Schrodinger LLC, which licenses the software used in this work.

■ ABBREVIATIONS

12*S*-HpETE, 12(*S*)-hydroperoxyeicosatetraenoic acid; 12*S*-HETE, 12(*S*)-hydroxyeicosatetraenoic acid; 13-HpODE, 13*S*-hydroperoxyoctadeca-9*Z*,11*E*-dienoic acid; 13-HODE, 13*S*-hydroxyoctadeca-9*Z*,11*E*-dienoic acid; AA, arachidonic acid; BSA, bovine serum albumin; c11-LOX, coral 11*R*-LOX; COX, cyclooxygenase; coxibs, COX-2-selective inhibitors; DCM, dichloromethane; E_{cat}, catalytically active enzyme; E_{apo}, inactive Fe-free enzyme; h12-LOX, human platelet 12*S*-lipoxygenase; h15-LOX-2, human epithelial 15-lipoxygenase-2; HDX-MS, hydrogen−deuterium exchange-mass spectrometry; ICP-MS, inductively coupled plasma mass spectrometer; LOX, lipoxygenase; ML355, h12-LOX specific inhibitor; NSAIDs, nonsteroidal anti-inflammatory drugs; PLAT, polycystin-1, lipoxygenase, α-toxin; PDZ, PSD95, Dig1, Zo-1; r15-LOX-1, r12/15-LOX, or rALOX15, rabbit 15S-LOX-1; SLO-1, soybean lipoxygense-1; SAXS, small-angle X-ray scattering; SEC, size exclusion chromatography; TOP, subdomain region in the helical bundle of the catalytic domain (residues 163−222); wt-h12-LOX, wild-type human platelet 12*S*-lipoxygenase.

■ REFERENCES

(1) Brash, A. R. (1999) Lipoxygenases: Occurrence, Functions, Catalysis and Acquisition of Substrate. *J. Biol. Chem. 274*, 23679−23682.

(2) Kuhn, H., Saam, J., Eibach, S., Holzhutter, H. G., Ivanov, I., and Walther, M. (2005) Structural biology of mammalian lipoxygenases: enzymatic consequences of targeted alterations of the protein structure. *Biochem. Biophys. Res. Commun. 338*, 93−101.

(3) Newcomer, M. E., and Brash, A. R. (2015) The structural basis for specificity in lipoxygenase catalysis. *Protein Sci. 24*, 298−309.

(4) Kagan, V. E., Mao, G., Qu, F., Angeli, J. P., Doll, S., Croix, C. S., Dar, H. H., Liu, B., Tyurin, V. A., Ritov, V. B., Kapralov, A. A., Amoscato, A. A., Jiang, J., Anthonymuthu, T., Mohammadyani, D., Yang, Q., Proneth, B., Klein-Seetharaman, J., Watkins, S., Bahar, I., Greenberger, J., Mallampalli, R. K., Stockwell, B. R., Tyurina, Y. Y., Conrad, M., and Bayir, H. (2017) Oxidized arachidonic and adrenic PEs navigate cells to ferroptosis. *Nat. Chem. Biol. 13*, 81−90.

(5) Drefs, M., Thomas, M. N., Guba, M., Angele, M. K., Werner, J., Conrad, M., Steib, C. J., Holdt, L. M., Andrassy, J., Khandoga, A., and Rentsch, M. (2017) Modulation of Glutathione Hemostasis by Inhibition of 12/15-Lipoxygenase Prevents ROS-Mediated Cell Death after Hepatic Ischemia and Reperfusion. *Oxid. Med. Cell. Longevity 2017*, 8325754.

(6) Friedmann Angeli, J. P., Schneider, M., Proneth, B., Tyurina, Y. Y., Tyurin, V. A., Hammond, V. J., Herbach, N., Aichler, M., Walch, A., Eggenhofer, E., Basavarajappa, D., Radmark, O., Kobayashi, S., Seibt, T., Beck, H., Neff, F., Esposito, I., Wanke, R., Forster, H., Yefremova, O., Heinrichmeyer, M., Bornkamm, G. W., Geissler, E. K., Thomas, S. B., Stockwell, B. R., O'Donnell, V. B., Kagan, V. E., Schick, J. A., and Conrad, M. (2014) Inactivation of the ferroptosis regulator Gpx4 triggers acute renal failure in mice. *Nat. Cell Biol. 16*, 1180−1191.

(7) Toppo, S., Flohe, L., Ursini, F., Vanin, S., and Maiorino, M. (2009) Catalytic mechanisms and specificities of glutathione peroxidases: variations of a basic scheme. *Biochim. Biophys. Acta, Gen. Subj. 1790*, 1486−1500.

(8) Tourdot, B. E., and Holinstat, M. (2017) Targeting 12-Lipoxygenase as a Potential Novel Antiplatelet Therapy. *Trends Pharmacol. Sci. 38*, 1006−1015.

(9) Hussain, H., Shornick, L. P., Shannon, V. R., Wilson, J. D., Funk, C. D., Pentland, A. P., and Holtzman, M. J. (1994) Epidermis Contains Platlet-Type 12-Lipoxygenase that is Overexpressed in Germinal Layer Keratinocytes in Psoriasis. *Am. J. Physiol. 266*, C243−C253.

(10) Ma, K., Nunemaker, C. S., Wu, R., Chakrabarti, S. K., Taylor-Fishwick, D. A., and Nadler, J. L. (2010) 12-Lipoxygenase Products Reduce Insulin Secretion and {beta}-Cell Viability in Human Islets. *J. Clin. Endocrinol. Metab. 95*, 887−893.

(11) Tersey, S. A., Bolanis, E., Holman, T. R., Maloney, D. J., Nadler, J. L., and Mirmira, R. G. (2015) Minireview: 12-Lipoxygenase and Islet beta-Cell Dysfunction in Diabetes. *Mol. Endocrinol. 29*, 791−800.

(12) Semeraro, M. L., Glenn, L. M., and Morris, M. A. (2017) The Four-Way Stop Sign: Viruses, 12-Lipoxygenase, Islets, and Natural Killer Cells in Type 1 Diabetes Progression. *Front. Endocrinol. (Lausanne, Switz.) 8*, 246.

(13) Connolly, J. M., and Rose, D. P. (1998) Enhanced angiogenesis and growth of 12-lipoxygenase gene-transfected MCF-7 human breast cancer cells in athymic nude mice. *Cancer Lett. 132*, 107−112.

(14) Natarajan, R., and Nadler, J. (1998) Role of lipoxygenases in breast cancer. *Front. Biosci., Landmark Ed. 3*, e81.

(15) Ding, X. Z., Iversen, P., Cluck, M. W., Knezetic, J. A., and Adrian, T. E. (1999) Lipoxygenase inhibitors abolish proliferation of human pancreatic cancer cells. *Biochem. Biophys. Res. Commun. 261*, 218−223.

(16) Shappell, S. B., Olson, S. J., Hannah, S. E., Manning, S., Roberts, R. L., Masumori, N., Jisaka, M., Boeglin, W. E., Vader, V., Dave, D. S., Shook, M. F., Thomas, T. Z., Funk, C. D., Brash, A. R., and Matusik, R. J. (2003) Elevated expression of 12/15-lipoxygenase and cyclooxygenase-2 in a transgenic mouse model of prostate carcinoma. *Cancer Res. 63*, 2256−2267.

(17) Guo, A. M., Liu, X., Al-Wahab, Z., Maddippati, K. R., Ali-Fehmi, R., Scicli, A. G., and Munkarah, A. R. (2011) Role of 12-lipoxygenase in regulation of ovarian cancer cell proliferation and survival. *Cancer Chemother. Pharmacol. 68*, 1273−1283.

(18) Prasad, V. V., Kolli, P., and Moganti, D. (2011) Association of a functional polymorphism (Gln261Arg) in 12-lipoxygenase with breast cancer. *Exp. Ther. Med. 2*, 317−323.

(19) Dailey, L. A., and Imming, P. (1999) 12-Lipoxygenase: Classification, Possible Therapeutic Benefits from Inhibition and Inhibitors. *Curr. Med. Chem. 6*, 389−398.

(20) Berglund, L., Bjorling, E., Oksvold, P., Fagerberg, L., Asplund, A., Al-Khalili Szigyarto, C., Persson, A., Ottosson, J., Wernerus, H., Nilsson, P., Lundberg, E., Sivertsson, A., Navani, S., Wester, K., Kampf, C., Hober, S., Ponten, F., and Uhlen, M. (2008) A genecentric Human Protein Atlas for expression profiles based on antibodies. *Mol. Cell. Proteomics 7*, 2019−2027.

(21) Sidhu, R. S., Lee, J. Y., Yuan, C., and Smith, W. L. (2010) Comparison of cyclooxygenase-1 crystal structures: cross-talk between monomers comprising cyclooxygenase-1 homodimers. *Biochemistry 49*, 7069−7079.

(22) Dong, L., Vecchio, A. J., Sharma, N. P., Jurban, B. J., Malkowski, M. G., and Smith, W. L. (2011) Human cyclooxygenase-2 is a sequence homodimer that functions as a conformational heterodimer. *J. Biol. Chem. 286*, 19035−19046.

(23) Gillmor, S. A., Villasenor, A., Fletterick, R., Sigal, E., and Browner, M. (1997) The structure of mammalian 15-lipoxygenase reveals similarity to the lipases and the determinants of substrate specificity. *Nat. Struct. Biol. 4*, 1003−1009.

https://dx.doi.org/10.1021/acs.biochem.1c00053
Biochemistry 2021, 60, 802−812

(24) Choi, J., Chon, J. K., Kim, S., and Shin, W. (2008) Conformational flexibility in mammalian 15S-lipoxygenase: Reinterpretation of the crystallographic data. *Proteins: Struct., Funct., Genet. 70*, 1023−1032.
(25) Ivanov, I., Shang, W., Toledo, L., Masgrau, L., Svergun, D. I., Stehling, S., Gómez, H., Di Venere, A., Mei, G., Lluch, J. M., Skrzypczak-Jankun, E., González-Lafont, À., and Kühn, H. (2012) Ligand-induced formation of transient dimers of mammalian 12/15-lipoxygenase: A key to allosteric behavior of this class of enzymes? *Proteins: Struct., Funct., Genet. 80*, 703−712.
(26) Neau, D. B., Gilbert, N. C., Bartlett, S. G., Boeglin, W., Brash, A. R., and Newcomer, M. E. (2009) The 1.85 A structure of an 8R-lipoxygenase suggests a general model for lipoxygenase product specificity. *Biochemistry 48*, 7906−7915.
(27) Gilbert, N. C., Bartlett, S. G., Waight, M. T., Neau, D. B., Boeglin, W. E., Brash, A. R., and Newcomer, M. E. (2011) The structure of human 5-lipoxygenase. *Science 331*, 217−219.
(28) Oldham, M. L., Brash, A. R., and Newcomer, M. E. (2005) Insights from the X-ray crystal structure of coral 8R-lipoxygenase: calcium activation via a C2-like domain and a structural basis of product chirality. *J. Biol. Chem. 280*, 39545−39552.
(29) Kobe, M. J., Neau, D. B., Mitchell, C. E., Bartlett, S. G., and Newcomer, M. E. (2014) The structure of human 15-lipoxygenase-2 with a substrate mimic. *J. Biol. Chem. 289*, 8562−8569.
(30) Aleem, A. M., Jankun, J., Dignam, J. D., Walther, M., Kuhn, H., Svergun, D. I., and Skrzypczak-Jankun, E. (2008) Human platelet 12-lipoxygenase, new findings about its activity, membrane binding and low-resolution structure. *J. Mol. Biol. 376*, 193−209.
(31) Eek, P., Poldemaa, K., Kasvandik, S., Jarving, I., and Samel, N. (2017) A PDZ-like domain mediates the dimerization of 11R-lipoxygenase. *Biochim. Biophys. Acta, Mol. Cell Biol. Lipids 1862*, 1121−1128.
(32) Aleem, A. M., Wells, L., Jankun, J., Walther, M., Kuhn, H., Reinartz, J., and Skrzypczak-Jankun, E. (2009) Human platelet 12-lipoxygenase: naturally occurring Q261/R261 variants and N544L mutant show altered activity but unaffected substrate binding and membrane association behavior. *Int. J. Mol. Med. 24*, 759−764.
(33) Shang, W., Ivanov, I., Svergun, D. I., Borbulevych, O. Y., Aleem, A. M., Stehling, S., Jankun, J., Kuhn, H., and Skrzypczak-Jankun, E. (2011) Probing dimerization and structural flexibility of mammalian lipoxygenases by small-angle X-ray scattering. *J. Mol. Biol. 409*, 654−668.
(34) Amagata, T., Whitman, S., Johnson, T. A., Stessman, C. C., Loo, C. P., Lobkovsky, E., Clardy, J., Crews, P., and Holman, T. R. (2003) Exploring sponge-derived terpenoids for their potency and selectivity against 12-human, 15-human, and 15-soybean lipoxygenases. *J. Nat. Prod. 66*, 230−235.
(35) Segraves, E. N., and Holman, T. R. (2003) Kinetic investigations of the rate-limiting step in human 12- and 15-lipoxygenase. *Biochemistry 42*, 5236−5243.
(36) Luci, D. K., Jameson, J. B., Yasgar, A., Diaz, G., Joshi, N., Kantz, A., Markham, K., Perry, S., Kuhn, N., Yeung, J., Kerns, E. H., Schultz, L., Holinstat, M., Nadler, J. L., Taylor-Fishwick, D. A., Jadhav, A., Simeonov, A., Holman, T. R., and Maloney, D. J. (2014) Synthesis and Structure-Activity Relationship Studies of 4-((2-Hydroxy-3-methoxybenzyl)amino)benzenesulfonamide Derivatives as Potent and Selective Inhibitors of 12-Lipoxygenase. *J. Med. Chem. 57*, 495−506.
(37) Pierce, B. G., Wiehe, K., Hwang, H., Kim, B. H., Vreven, T., and Weng, Z. (2014) ZDOCK server: interactive docking prediction of protein-protein complexes and symmetric multimers. *Bioinformatics 30*, 1771−1773.
(38) Pascal, B. D., Willis, S., Lauer, J. L., Landgraf, R. R., West, G. M., Marciano, D., Novick, S., Goswami, D., Chalmers, M. J., and Griffin, P. R. (2012) HDX Workbench: softwared for the analysis of H/D exchange MS data. *J. Am. Soc. Mass Spectrom. 23*, 1512−1521.
(39) Hoofnagle, A. N., Resing, K. A., and Ahn, N. G. (2003) Protein analysis by hydrogen exchange mass spectrometry. *Annu. Rev. Biophys. Biomol. Struct. 32*, 1−25.
(40) Luci, D. K., Jameson, J. B., Yasgar, A., Diaz, G., Joshi, N., Kantz, A., Markham, K., Perry, S., Kuhn, N., Yeung, J., Kerns, E. H., Schultz, L., Holinstat, M., Nadler, J. L., Taylor-Fishwick, D. A., Jadhav, A., Simeonov, A., Holman, T. R., and Maloney, D. J. (2014) Synthesis and Structure-Activity Relationship Studies of 4-((2-Hydroxy-3-methoxybenzyl)amino)benzenesulfonamide Derivatives as Potent and Selective Inhibitors of 12-Lipoxygenase. *J. Med. Chem. 57*, 495−506.
(41) Englander, S. W. (2006) Hydrogen exchange and mass spectrometry: a historical perspective. *J. Am. Soc. Mass Spectrom. 17*, 1481−1489.
(42) Konermann, L., Pan, J., and Liu, Y.-H. (2011) Hydrogen exchange mass spectrometry for studying protein structure and dynamics. *Chem. Soc. Rev. 40*, 1224−1234.
(43) Pirrone, G. F., Iacob, R. E., and Engen, J. R. (2015) Applications of hydrogen/deuterium exchange MS from 2012 to 2014. *Anal. Chem. 87*, 99−118.
(44) Droege, K. D., Keithly, M. E., Sanders, C. R., Armstrong, R. N., and Thompson, M. K. (2017) Structural dynamics of 15-lipoxygenase-2 via hydrogen-deuterium exchange. *Biochemistry 56*, 5065−5074.
(45) Offenbacher, A. R., and Holman, T. R. (2020) Fatty acid allosteric regulation of C-H activation in plant and animal lipoxygenases. *Molecules 25*, 3374.
(46) Aleem, A. M., Tsai, W.-C., Tena, J., Alvarez, G., Deschamps, J., Kalyanaraman, C., Jacobson, M. P., and Holman, T. R. (2019) Probing the electrostatic and steric requirements for substrate binding in human platelet-type 12-lipoxygenase. *Biochemistry 58*, 848−857.
(47) Knapp, M. J., Rickert, K., and Klinman, J. P. (2002) Temperature-dependent isotope effects in soybean lipoxygenase-1: correlating hydrogen tunneling with protein dynamics. *J. Am. Chem. Soc. 124*, 3865−3874.
(48) Hu, S., Offenbacher, A. R., Thompson, E. M., Gee, C. L., Wilcoxen, J., Carr, C. A. M., Prigozhin, D. M., Yang, V., Alber, T., Britt, R. D., Fraser, J. S., and Klinman, J. P. (2019) Biophysical characterization of a disabled double mutant of soybean lipoxygenase: the 'undoing' of precise substrate positioning relative to metal cofactor and an identified dynamical network. *J. Am. Chem. Soc. 141*, 1555−1567.
(49) Offenbacher, A. R., Hu, S., Poss, E. M., Carr, C. A. M., Scouras, A. D., Prigozhin, D. M., Iavarone, A. T., Palla, A., Alber, T., Fraser, J. S., and Klinman, J. P. (2017) Hydrogen-deuterium exchange of lipoxygenase uncovers a relationship between distal, solvent exposed protein motions and the thermal activation barrier for catalytic proton-coupled electron tunneling. *ACS Cent. Sci. 3*, 570−579.
(50) Newie, J., Neumann, P., Werner, M., Mata, R. A., Ficner, R., and Feussner, I. (2017) Lipoxygenase 2 from Cyanothece sp. controls dioxygen insertion by steric shielding and substrate fixation. *Sci. Rep. 7*, 2069.
(51) Lella, M., and Mahalakshmi, R. (2017) Metamorphic Proteins: Emergence of Dual Protein Folds from One Primary Sequence. *Biochemistry 56*, 2971−2984.
(52) Yeung, J., Tourdot, B. E., Fernandez-Perez, P., Vesci, J., Ren, J., Smyrniotis, C. J., Luci, D. K., Jadhav, A., Simeonov, A., Maloney, D. J., Holman, T. R., McKenzie, S. E., and Holinstat, M. (2014) Platelet 12-LOX is essential for FcgammaRIIa-mediated platelet activation. *Blood 124*, 2271−2279.
(53) Deschamps, J. D., Gautschi, J. T., Whitman, S., Johnson, T. A., Gassner, N. C., Crews, P., and Holman, T. R. (2007) Discovery of platelet-type 12-human lipoxygenase selective inhibitors by high-throughput screening of structurally diverse libraries. *Bioorg. Med. Chem. 15*, 6900−6908.
(54) Suzuki, H., Kishimoto, K., Yoshimoto, T., Yamamoto, S., Kanai, F., Ebina, Y., Miyatake, A., and Tanabe, T. (1994) Site-directed mutagenesis studies on the iron-binding domain and the determinant for the substrate oxygenation site of porcine leukocyte arachidonate 12-lipoxygenase. *Biochim. Biophys. Acta, Lipids Lipid Metab. 1210*, 308−316.

https://dx.doi.org/10.1021/acs.biochem.1c00053
Biochemistry 2021, 60, 802−812